Controlled supercontinuum generation for optimal pulse compression

Spanner, M; Pshenitchnikov, Maxim; Olvo, [No Value]; Ivanov, M

IMPORTANT NOTE: You are advised to consult the publisher's version (publisher's PDF) if you wish to cite from it. Please check the document version below.

Document Version
Publisher's PDF, also known as Version of record

[Link to publication in University of Groningen/UMCG research database](#)

M. SPANNER[1,2]
M. PSHENICHNIKOV[3]
V. OLVO[4]
M. IVANOV[2,✉]

Controlled supercontinuum generation for optimal pulse compression: a time-warp analysis of nonlinear propagation of ultra-broad-band pulses

[1] Department of Physics, University of Waterloo, Waterloo, Ontario N2L 3G1, Canada

[2] Steacie Institute for Molecular Sciences, NRC Canada, 100 Sussex Drive, Ottawa, Ontario K1A 0R6, Canada

[3] Ultrafast Laser and Spectroscopy Laboratory, Materials Science Centre, Department of Chemistry, University of Groningen, The Netherlands

[4] Center for Advanced Research, 1553 Aline Avenue, Orleans, Ontario K4A 3Z2, Canada

ABSTRACT We describe the virtues of the pump–probe approach for controlled supercontinuum generation in nonlinear media, using the example of pulse compression by cross-phase modulation in dielectrics. Optimization of a strong (pump) pulse and a weak (probe) pulse at the input into the medium opens the route to effective control of the supercontinuum phases at the output. We present an approximate semi-analytical approach which describes nonlinear transformation of the input pulse into the output pulse. It shows how the input and the output chirps are connected via a time-warp transformation which is almost independent of the shape of the probe pulse. We then show how this transformation can be used to optimize the supercontinuum generation to produce nearly single-cycle pulses tunable from mid-infrared to ultraviolet.

PACS 42.65.Re; 42.65.Ky

1 Introduction

Extreme spectral broadening of intense pulses propagating in nonlinear media is a basis for generating ultra-short pulses and supercontinua with applications ranging from controlling quantum dynamics to standards.

Analysis of the interplay of self- and cross-phase modulation (SPM and XPM), self-steepening, dispersion, wave mixing, etc. [1, 2] during the propagation of intense ultra-short pulses is a challenging problem. For such pulses the familiar slowly varying envelope approximation (SVEA) breaks down [3]. The standard second-order Taylor expansion of the medium dispersion around the carrier frequency is unwarranted. The concept of the carrier frequency for octave-wide spectra becomes ambiguous. Analytical solutions appear to be impossible and repeated numerical simulations for a variety of input pulses are usually needed to obtain a comprehensive physical picture. Any optimization problem such as pulse compression, where one looks for the best input pulse to match the desired frequency-converted output after the non-

linear medium, appears even more difficult: a very large number of trial pulses is required for the convergence of standard iterative search algorithms.

We show that, contrary to this first impression, strong dispersion combined with nonlinearity and large bandwidth allow for semi-analytical solutions and a substantial simplification of the analysis. For standard approaches to spectral broadening, especially those based on XPM [4], molecular phase modulation (MPM) [5–7] and – within certain important restrictions – SPM, it is possible to define an effective response function for the medium which is almost independent of the input pulse. Then the result of nonlinear propagation of many trial pulses can be obtained as a simple, easily visualized transformation. This allows us to quickly analyze the degree to which one can control phases of the supercontinuum at the output of a nonlinear medium by optimizing the input into the medium.

Flexible engineering of the output phases across the supercontinuum spectrum is the most critical part of pulse compression. In standard pulse-compression schemes [8–11], where supercontinuum is generated starting with SPM of an intense laser pulse, required phase adjustments are done at the output of the medium, usually using spatial light modulators or acousto-optic modulators [12, 13]. As the output bandwidth grows, the adjustment of the output phases becomes more demanding. From the pulse-shaping perspective alone, it would be much easier to shape the narrow spectrum at the input rather than the octave-wide (or broader) spectrum at the output. The pulse-compression approach proposed below allows one to do exactly that: move the required shaping to the input spectrum.

In our approach, a strong pump pulse induces a nonlinear response of the medium. A weaker probe pulse scatters off the induced nonlinear polarization. The intensity of the probe is limited by the requirement that the probe does not change the nonlinear response of the medium induced by the strong pump. This setup decouples the medium response from the details of the probe pulse being compressed. The probe can then be pre-shaped at the input [14]. Shaping can include precompensation for dispersion in the medium and in the optical elements after the medium, to all orders. With the pump pulse held constant, the probe propagation is almost linear [16].

✉ Fax: +1-613/993-3437, E-mail: misha.ivanov@nrc.ca

Therefore, small changes at the input do not lead to large changes at the output, making the optimization robust. Furthermore, the pump–probe approach also allows one to easily tune the output spectrum by keeping the pump wavelength fixed while tuning the probe wavelength at the input.

As an example, we consider the scheme where a strong pump pulse and a weak probe pulse are sent through a thin piece of dielectric; see Fig. 1. The pulses propagate at a small angle: nearly collinear inside the glass, they spatially separate afterward. The pump is fixed, say at 800 nm, while the probe is tunable. Both pulses can be shaped at the input, with the goal of maximum compression of the probe down to one or two cycles at the output. Dispersion is used as a part of the compression scheme.

Motivated by practical considerations, we almost always constrain the pump pulse to a single-peaked envelope with no chirp underneath. The only exception is the compression of a UV probe, where very high dispersion in glasses has forced us to allow for a double-peaked envelope of the pump, still without any initial chirp.

In our previous publication [17] we have shown how this XPM-based approach can be used to compress pulses down to one or two optical cycles tunable from UV to mid-IR. A similar idea can be applied to MPM in hollow fibers [14, 15], where the compression is even better due to weaker dispersion. Here, we concentrate on the detailed description of the semi-analytical optimization procedure. Using the example of XPM in dielectric materials, we show how the semi-analytical analysis can be used to find the limits and the optimal region of the compression. Full numerical calculations are then used to fine-tune the initial guess provided by the analytical analysis.

The numerical simulations include the Kerr and the Raman responses of the glass [1], cascade wave-mixing processes whenever important, dispersion, and self-steepening. Thin glasses (typically less than 1 mm) and the assumption of loose focusing allow us to use 1D propagation and neglect pulse filamentation and self-focusing.

The paper is organized as follows. In Sect. 2 we present the numerical model and approximate semi-analytical results
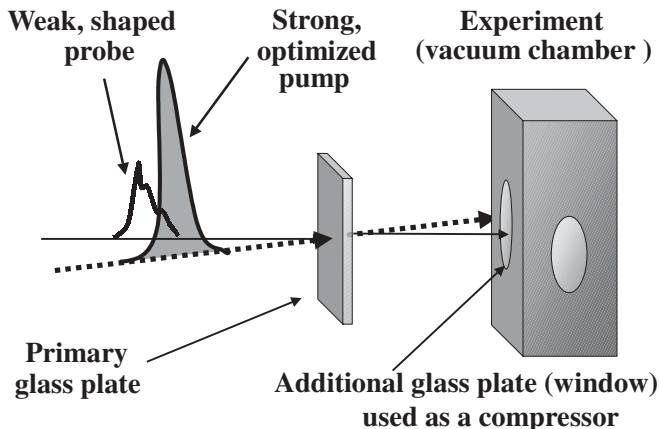
which describe the transformation of the input pulse and introduce the time-warp function. We complete Sect. 2 with a detailed recipe describing how the time-warp analysis can be used to evaluate the controllability of the generated supercontinuum and to find the optimal regime for achieving a desired target (in our case, pulse compression). Section 3 illustrates the application of the time-warp analysis, using pulse compression as an example of the optimization problem. A step-by-step description of the time-warp analysis is accompanied by full numerical simulations.

2 Semi-analytical and computational models

A numerical search for an optimal regime of supercontinuum generation, e.g. with the eventual goal of pulse compression, resembles searching for a needle in a haystack. The semi-analytical model described below provides a basis for the first-order analysis of the supercontinuum generation. Loosely speaking, it points to the corner of the haystack where the needle (optimal solution) resides.

Experimentally, a search for the optimal solution can be done very efficiently using feedback-based algorithms, in which a measurement of an output pulse vs. the desired target is fed back to the input to modify the next trial pulse, until the desired target is approximated with sufficient precision. A specific version of such closed-loop search algorithms, genetic algorithms, has been successfully used in many applications other than pulse compression: optimization of laser-induced fluorescence [18], high-harmonic generation [19], molecular dynamics and photochemical reactions [20–23], etc. Recently, Omenetto et al. used adaptive pulse shaping to suppress unwanted nonlinear effects [24], so that pulse propagation in fibers over long distances would not suffer from self-induced nonlinearities.

Finding an optimal solution may take many tens or even hundreds of thousand of trial pulses, but with kHz or even MHz repetition rates of modern lasers the search is over in a matter of minutes.

Theoretically, the situation is completely different. Propagating each trial pulse through the nonlinear medium on the computer takes much longer (many orders of magnitude longer) than in the laboratory. In this case, a theoretician does not have the luxury of running tens of thousands of trial pulses. A blind search must be replaced with a more intelligent procedure. One possible approach is described in Sect. 2.2.

2.1 Numerical model

Without using the slowly varying envelope approximation (SVEA), in the frequency domain the Maxwell equation can be reduced to (see e.g. [25] or the derivation in Appendix A below):

$$\left[\frac{\partial}{\partial x} - i\frac{\omega}{c}n(\omega)\right] E(x, \omega) = \frac{2\pi}{cn(\omega)}i\omega P_{NL}(x, \omega). \qquad (1)$$

Here $E(x, \omega)$ is the Fourier transform of the electric field $\mathcal{E}(x, t)$, P_{NL} is the nonlinear polarization per unit volume, and $n(\omega)$ is the linear refractive index. Here we restrict ourselves

FIGURE 1 Scheme for pulse compression using XPM with optimization of the pulses at the input. Two pulses, one (probe) weaker than the other (pump), are loosely focused into a nonlinear medium – a transparent dielectric such as fused silica or CaF$_2$. The pulses propagate at a small angle, so that they spatially separate in the far field. Both pulses are optimized to compress the weaker pulse inside the vacuum chamber

Labels in figure: Weak, shaped probe · Strong, optimized pump · Experiment (vacuum chamber) · Primary glass plate · Additional glass plate (window) used as a compressor

to the 1D case, which is justified by the loose-focusing geometry and thin glasses.

For the numerical solution we use the time-domain version of (1):

$$\frac{\partial \mathcal{E}(x,t)}{\partial x} + \frac{1}{c}\frac{\partial}{\partial t}\widehat{\mathrm{FT}}^{-1}\left[n(\omega)E(x,\omega) + 2\pi\frac{P_{\mathrm{NL}}(x,\omega)}{n(\omega)}\right] = 0\,,$$

$$(2)$$

where $\widehat{\mathrm{FT}}^{-1}$ means inverse Fourier transform.

Note that any complex electric field $\mathcal{E}(x,t)$ can be written as

$$\mathcal{E}(x,t) = F(x,t)\exp\left(-\mathrm{i}\varphi(x,t)\right).$$

$$(3)$$

Here F, φ are the time-dependent amplitude and phase of the complex field $\mathcal{E}(x,t)$.

Equation 2 is first solved for the strong pump pulse $\mathcal{E}_{\mathrm{s}} = F_{\mathrm{s}}\exp\left(-\mathrm{i}\varphi_{\mathrm{s}}\right)$, in which case $\widehat{\mathrm{FT}}^{-1}\left[2\pi P_{\mathrm{NL}}(x,\omega)/n(\omega)\right]$ is set to $n_2 F_{\mathrm{s}}^2\mathcal{E}_{\mathrm{s}}$. The pump field $\mathcal{E}_{\mathrm{s}}$ and the pump-induced nonlinearity $2n_2 F_{\mathrm{s}}^2$ acting on the weak probe field $\mathcal{E}_{\mathrm{w}}$ are recorded along the propagation length and are used as inputs to calculate the propagation of the probe pulse.

In the case of XPM one might need to be careful with the cascade wave-mixing processes, which start with the generation of the new field with frequency ω_{c} and wave vector $\boldsymbol{k}_{\mathrm{c}}$:

$$\omega_{\mathrm{c}} = \omega_{\mathrm{s}} + \omega_{\mathrm{s}} - \omega_{\mathrm{w}} \neq \omega_{\mathrm{PR}}\,,$$

$$\boldsymbol{k}_{\mathrm{c}} = \boldsymbol{k}_{\mathrm{s}} + \boldsymbol{k}_{\mathrm{s}} - \boldsymbol{k}_{\mathrm{w}}\,.$$

$$(4)$$

Here the subscript 's' denotes strong pump field, the subscript 'w' denotes weak probe field, and the subscript 'c' denotes the first wave in the cascade wave-mixing sequence. The field ω_{c}, $\boldsymbol{k}_{\mathrm{c}}$ can in turn mix with the pump to generate the field with frequency and wave vector equal to those of the probe, etc.

Due to the geometry of the problem (see Fig. 1) the waves $\boldsymbol{k}_{\mathrm{s}}$, $\boldsymbol{k}_{\mathrm{w}}$, $\boldsymbol{k}_{\mathrm{c}}$ all propagate in different directions and these cascade wave-mixing processes are generally not phase matched. We ignore them unless the pump and the probe have similar input wavelength, i.e. ~ 800 nm. In this latter case the cascade processes are included in the numerical calculation. We find that, while for a given input the output is somewhat changed, the cascade processes virtually do not affect the results of the optimization procedure. In fact, we found that the optimal output pulses were even somewhat shorter when the cascade processes were included for the case of a 800-nm probe (the pump is fixed at 800 nm).

To solve (2), we go to the moving frame $t' = t - x/v_{\mathrm{s}}$, where v_{s} is the group velocity with which the pump pulse propagates. The wave equation can be written as

$$\frac{\partial E}{\partial x} = \widehat{\mathcal{L}}E\,,$$

$$(5)$$

where the operator $\widehat{\mathcal{L}}$ includes direct and inverse Fourier transforms between the time and frequency domains as seen in (2). The pulse is specified for all times at the initial x position

and is then propagated by standard finite-difference methods:

$$E\big|_{x+1}^{t} = E\big|_{x-1}^{t} + 2\Delta_x\widehat{\mathcal{L}}E\big|_{x}^{t}\,,$$

$$(6)$$

where Δ_x is the step size in the x direction. The first step in x is executed using a simple forward-difference representation:

$$E\big|_{x=1}^{t} = E\big|_{x=0}^{t} + \Delta_x\widehat{\mathcal{L}}E\big|_{x=0}^{t}\,.$$

$$(7)$$

2.2 *Time warp, frequency map, and optimization*

The first step in our semi-analytical approach is to simplify the inverse transform of (1) back to the time domain. We begin by writing $\mathcal{E}(t)$ as

$$\mathcal{E}(t) = F(t)\exp\left(-\mathrm{i}\varphi(t)\right).$$

$$(8)$$

Due to dispersion and nonlinearity in the medium the broadband pulse becomes strongly chirped. Even though its spectrum can be broad, due to the strong chirp the amplitude F would usually be a slower function of time compared to $\exp(-\mathrm{i}\varphi)$, with the phase $\varphi(t)$ depending nonlinearly on time. At any given time, the instantaneous frequency of the pulse,

$$\omega(t) = \mathrm{d}\varphi(t)/\mathrm{d}t \equiv \dot{\varphi}(t)\,,$$

$$(9)$$

is well defined. It is this strong chirp which allows one to simplify the Fourier transform of (1) back to the time domain. The approach breaks down when one runs into catastrophic self-steepening and F develops a shock-wave front (or rear end), or when the strong chirp is simply not there.

To make the discussion both simpler and more specific, we will restrict ourselves to nonlinearities of the type $n_2 F^2$, where n_2 is the nonlinear part of the refractive index. In the case of XPM, the nonlinearity is $2n_2 F_{\mathrm{s}}^2$, where F_{s} is the amplitude of the strong (pump) pulse, and for SPM it is $n_2 F_{\mathrm{s}}^2$. Generalization of the results to the case of Raman excitation and MPM is rather straightforward. Full numerical analysis should, of course, include all other important contributions to nonlinear polarization, such as Raman response and the cascade wave-mixing processes.

Usually, for the inverse Fourier transform of $n(\omega)E(\omega)$ in (1) back to the time domain, one expands $n(\omega)$ in Taylor series to the second order:

$$n(\omega) \approx n_0 + \omega n' + \frac{1}{2!}n''\omega^2.$$

$$(10)$$

Here primes denote derivatives with respect to the whole argument. In our case of a broad spectrum $n(\omega)$ should be expanded to all orders:

$$n(\omega) = n_0 + \omega n' + \frac{1}{2!}n''\omega^2 + \frac{1}{3!}n'''\omega^3 + \cdots\,,$$

$$(11)$$

and none can be neglected. The inverse Fourier transform of a term $\omega^k E(\omega)$ yields $\partial^k\mathcal{E}/\partial t^k = \left(\partial^k/\partial t^k\right)Fe^{-\mathrm{i}\varphi}$, and all of them (with $k \to \infty$) have to be included. At first glance, the situation seems rather grim.

Physically, the simplification comes from the fact that due to strong chirp different instantaneous frequencies $\omega(t) = \dot{\varphi}(t)$

arrive at different times (here the dot denotes time derivative). Hence, at any given time it is sufficient to know $n(\dot{\varphi}(t))$, $n'(\dot{\varphi}(t))$, and $n''(\dot{\varphi}(t))$ at the instantaneous frequency $\omega(t) \equiv \dot{\varphi}(t)$. That is, while the spectrum is very broad, at any given time local expansion of the refractive index around the instantaneous frequency is sufficient.

Mathematically, strong chirp means $\Delta\omega T \gg 1$, where $\Delta\omega$ is the bandwidth and T is the duration of the pulse. This allows us to write

$$\frac{\partial^k}{\partial t^k} F e^{-i\varphi} \approx (-i\dot{\varphi})^k F e^{-i\varphi} + (-i\dot{\varphi})^{k-1} k \dot{F} e^{-i\varphi}$$
$$+ \frac{k(k-1)}{2} (-i)^{k-1} (\dot{\varphi})^{k-2} \ddot{\varphi} F e^{-i\varphi}, \qquad (12)$$

where all terms with the derivatives of the amplitude F higher than $\dot{F}$ have been neglected compared to $\dot{\varphi}$.

While this approximation might be reminiscent of the slowly varying envelope approximation, the key difference is the appearance of the instantaneous (rather than the carrier) frequency $\omega(t) = \dot{\varphi}(t)$. This frequency may change significantly during the pulse; in the limit $\Delta\omega T \gg 1$ the range of its change determines the pulse bandwidth $\Delta\omega$. The amplitude $F(t)$ is not the same as the usual pulse envelope $A(t)$, which is frequently defined as $\mathcal{E}(t) = A(t) \exp(-i\omega_0 t)$ (ω_0 is the carrier frequency). In our case not only the carrier, but also all chirps – which could be quite large – are removed from $F(t)$.

After somewhat tedious but straightforward algebra and using $\Delta\omega T \gg 1$, the Fourier transform of (1) can be reduced to

$$\frac{\partial}{\partial x} F e^{-i\varphi} + \frac{1}{c} \frac{\partial}{\partial t} \left[n(\dot{\varphi}) + n_2 F^2 \right] F e^{-i\varphi}$$
$$+ \frac{i}{c} \frac{\partial}{\partial t} \left[n'(\dot{\varphi}) \dot{F} + \frac{1}{2} n''(\dot{\varphi}) \ddot{\varphi} F \right] e^{-i\varphi} = 0. \qquad (13)$$

While this is similar to the equation obtained with the usual second-order Taylor expansion of $n(\omega)$, the key difference is the instantaneous frequency $\dot{\varphi} = \omega(t)$: the expansion of $n(\omega)$ is always local near $\omega(t)$. Separating real and imaginary parts, we obtain

$$\frac{\partial}{\partial x} F + \frac{1}{c} \frac{\partial}{\partial t} \left[n_{gr}(\dot{\varphi}) + n_2 F^2 \right] F - \frac{1}{2c} F \left[\frac{\partial n_{gr}(\dot{\varphi})}{\partial t} \right] = 0,$$
$$\frac{\partial}{\partial x} \varphi + \frac{1}{c} \left[n(\dot{\varphi}) + n_2 F^2 \right] \frac{\partial}{\partial t} \varphi = 0, \qquad (14)$$

where $n_{gr}(\omega) \equiv n(\omega) + n'(\omega)\omega$. In the second equation we used the condition of strong chirp, $\Delta\omega T \gg 1$, to drop $\partial(n'F + 0.5n''F\ddot{\varphi})/\partial t$ compared to $nF\dot{\varphi}$. For a weak pulse in the case of XPM, the term $n_2 F^2$ is replaced by $2n_2 F_s^2$, where F_s is the amplitude of the strong pulse (pump).

Input into (14) are the time-dependent amplitude $F_{in}(t)$ and the time-dependent phase $\varphi_{in}(t)$ at the beginning of the medium, $x = 0$. The most important function at the output $x = L$ is the phase $\varphi_{out}(t) = \varphi(L, t)$.

Equations (14) suggest a two-step iterative scheme to analyze the transformation of the input pulses for various input chirps $\varphi_{in}(t)$, in the case of both SPM and XPM. Suppose that at the input into the nonlinear medium the pulse carrier frequency is ω_0. For the first iteration, we solve (14) (or

(1)) numerically only once for a constant input frequency ω_0, i.e. setting $\varphi_{in}^{(0)} = \omega_0 t$. We obtain $\varphi^{(0)}(x, t)$ and $F_s(x, t)$ everywhere in the medium, for a given input amplitude $F_{s,in}(t)$ of the strong pulse.

For the second iteration, we can substitute the solutions $F_s(x, t)$ and $\varphi^{(0)}(x, t)$ into (14), replacing $n(\dot{\varphi})$, $n_{gr}(\dot{\varphi})$ with $n(\dot{\varphi}^{(0)})$, $n_{gr}(\dot{\varphi}^{(0)})$. Now, $n(\dot{\varphi})$, $n_{gr}(\dot{\varphi})$, and the terms in the square brackets in (14) are all known, fixed functions of x, t as long as the amplitude of the strong pulse at the input $F_{s,in}$ is fixed.

This simple approximation immediately decouples the second of the equations (14) from the first, as long as the amplitude of the strong pulse at the input is fixed. Note that fixing the input amplitude of the pump while varying its time-dependent phase $\varphi_{in}(t)$ – which is what we will be doing if we are trying to control SPM – means that we will be dealing with different input spectra, i.e. with amplitude modulations at the input. Thus, for SPM the family of input–output transformations characterized by a single map function described below is somewhat unusual: members of the same family will have different input spectral amplitudes but similar time-domain envelopes $F_{in}(t)$.

With the fixed amplitude of the strong pulse, one can see that the propagation of an arbitrary input chirp (for either the pump or the probe) $\varphi_{in}(t) = \omega_0 f_{in}(t)$ is determined by a single time-warp transformation defined as

$$\tau(x, t') \equiv \varphi^{(0)}(x, t')/\omega_0. \qquad (15)$$

Here $t' = t - xn(\omega_0)/c$ is time in the co-propagating frame; remember that $\varphi^{(0)}(x, t')$ corresponds to $\varphi_{in} = \omega_0 t$. Indeed, one can check that for an arbitrary input $\varphi_{in}(t') = \omega_0 f_{in}(t')$ the solution of the desired propagation equation

$$\frac{\partial \varphi}{\partial x} + \frac{\Delta n(x, t')}{c} \frac{\partial \varphi}{\partial t'} = 0 \qquad (16)$$

(where $\Delta n(x, t') = n(\dot{\varphi}^{(0)}) + n_2 F^2(x, t') - n(\omega_0)$ for SPM or $\Delta n(x, t') = n(\dot{\varphi}^{(0)}) + 2n_2 F_s^2(x, t') - n(\omega_0)$ for XPM) is simply

$$\varphi(x, t') = \omega_0 f_{in} \left(\tau(x, t') \right). \qquad (17)$$

This statement becomes obvious when (17) is substituted into (16) and one recalls that $\tau(x, t') \equiv \varphi^{(0)}(x, t')/\omega_0$ satisfies (16) by definition: this is precisely where $\tau(x, t')$ was obtained from. The same applies to MPM where the change in the refractive index is determined by Raman excitation; this change for intense pump pulses is given in e.g. [15].

The result (17) allows us to introduce the frequency map $R(t')$ to characterize nonlinear transformation of the input frequency $\omega_{in}(t') = \omega_0 \dot{f}_{in}(t')$. Realizing that the instantaneous output frequency $\omega_{out}(t')$ is $d\varphi_{out}(t')/dt'$, where φ_{out} is given by (17), we see that

$$R(t') = \frac{\omega_{out}(t')}{\omega_{in}(t')} = \left[\frac{\dot{f}_{in} \left(\tau(t', L) \right)}{\dot{f}_{in}(t')} \right] \frac{\partial \tau(L, t')}{\partial t'}. \qquad (18)$$

The factor in square brackets is determined by the input chirp only and is close to unity for a sufficiently narrow input spectrum. The frequency map is dominated by $\partial\tau(L, t')/\partial t'$. The latter is determined from a single numerical solution of (1) for

a constant input frequency $\varphi_{\rm in} = \omega_0 t$ and is independent of the initial chirp. For negligible dispersion and a pre-set Raman excitation of the medium a similar frequency map is implicit in the results of [14, 26].

We can now summarize the approach to analyzing the supercontinuum.

1. First, one solves the Maxwell equations for a fixed instantaneous input frequency and amplitude of a strong pulse, using its time-domain representation $\mathcal{E}_{\rm s}(t) = F_{\rm s}(t) \times \exp\left(-\mathrm{i}\varphi_{\rm s}(t)\right)$. The solution is done in the co-propagating frame $t' = t - xn(\omega_0)/c$. This yields $\varphi(L, t')$ at the output;
2. Second, one obtains the time warp (15) and the frequency map $\partial\tau(L, t')/\partial t'$;
3. Third, for any initial chirp in the time domain, the output chirp, also in the time domain, can be obtained from (17); the range of frequencies at the output can be obtained from (18).

We stress that it turns out to be very convenient to use chirps in the time domain and base the analysis on instantaneous frequencies.

In Sect. 3.1 we give a detailed illustration of this approach for the specific case of pulse compression.

3   Compression by cross-phase modulation

In the XPM example considered here, a strong pump pulse and a weak probe pulse are sent through a thin piece of dielectric, as shown in Fig. 1. Depending on the probe wavelength, we use either CaF_2 or fused silica. The pump is fixed at 800 nm, while the probe is tunable: we consider wavelengths between 3 μm and 400 nm. Both pump and probe pulses can be shaped at the input, with the goal of maximum compression of the probe down to one or two cycles. We keep the shape of the pump as simple as possible. Dispersion in the glass, included to all orders, is used as a part of the compression scheme. An additional CaF_2 plate can be added after the nonlinear medium for the final compression of the probe pulse by a purely linear propagation.

As an illustration, consider the compression of a 3-μm probe pulse down to the single-cycle regime. As a target of the optimization procedure, we choose a near-single-cycle 15-fs pulse at 3 μm shown in Fig. 2a. Propagating this target pulse backwards through the additional CaF_2 plate, which serves as the final compressor and was chosen to be 1.5 mm thick, defines the target at the output of the nonlinear medium shown in Fig. 2b.
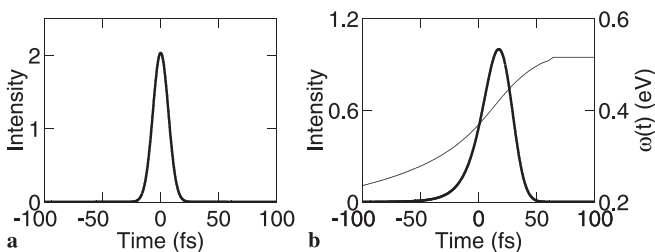
3.1   *Time-warp analysis and optimization*

The time-warp analysis can now be used to find the limits and the optimal conditions for generating such a pulse using XPM in glass.

Figure 3a shows the frequency map $\tau_{t'} \equiv \partial\tau/\partial t'$ for the propagation lengths of 0, 0.5, 1, and 1.2 mm. The pump pulse was $\mathcal{E}_{\rm s}(t) \propto \exp\left[-(t/\sigma)^2 - \mathrm{i}\omega_0 t\right]$, with $\sigma = 90$ fs and carrier wavelength of 800 nm (see Fig. 4a). The intensity of the pump was such that $n_2 F^2 = 3.2 \times 10^{-3}$ at the maximum of the field, for CaF_2 as a medium. For larger propagation lengths the function $\tau_{t'}$ grows in amplitude. If the propagation length is increased much beyond 1 mm (for the present case) the frequency map stops growing in amplitude and starts to 'smear' in the horizontal direction. This is due to dispersive effects of the medium.

The input probe pulse needed for compression to the near-single-cycle regime is found as follows. From the target 15-fs pulse, propagated backwards through the additional CaF_2 plate, we extract the instantaneous output frequency $\omega_{\rm out}(t)$ (see Fig. 3b). The straight lines denote the desired output bandwidth $\Delta\omega_{\rm out}(t)$ with the correct target chirp. Now, using (17) and the function $\tau_{t'}$, we can find the estimated target frequency at the input, $\omega_{\rm in}(t') = \omega_{\rm out}(t')/\tau_{t'}$. Panel c shows the calculated $\omega_{\rm in}(t)$ for the nonlinear medium length of 0.5 mm, while panel d shows $\omega_{\rm in}(t)$ for 1 mm and e corresponds to 1.2 mm. The dashed line in these panels re-plots the desired output frequency $\omega_{\rm out}(t)$.

FIGURE 2 Optimization target. **a** Target near-single-cycle transform-limited 3-μm pulse. **b** Target pulse after backwards propagation through the additional 1.5-mm CaF_2 plate. *Thin line* shows instantaneous frequency $\omega(t)$ in the time domain, which shows strong nonlinear chirp
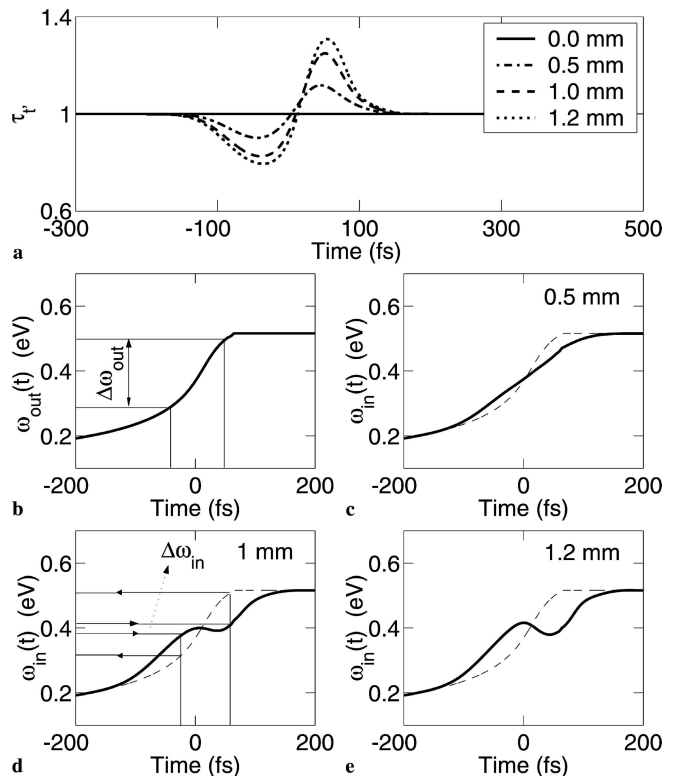
FIGURE 3 Time-warp analysis. **a** Frequency map $\tau_{t'}$ for a range of pump propagation lengths. **b** The desired output chirp of the probe pulse. **c–e** *Solid line*: the required input chirp of the probe pulse for a range of propagation lengths. *Dashed line*: the desired output chirp $\omega_{\rm out}(t)$ (see text for additional explanation)
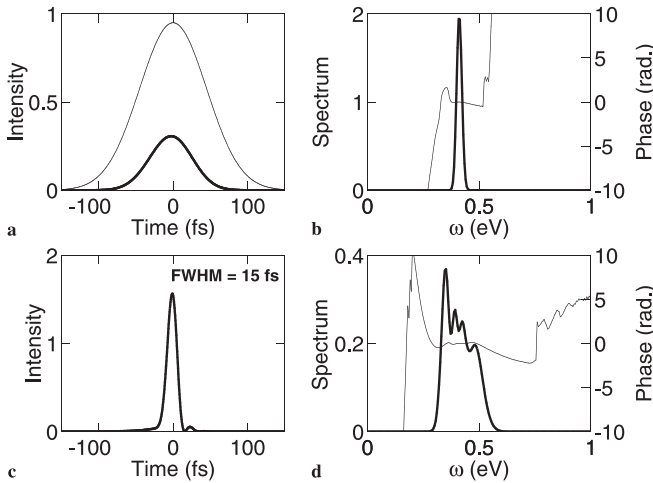
FIGURE 4 Compression of 3-μm probe pulse. **a** The intensity of the optimized probe (*thick*) and pump (*thin*) before the nonlinear medium. **b** Spectrum (*thick*) and phase (*thin*) of the probe in (a). **c** Intensity of compressed probe. **d** Spectrum and phase of compressed probe

It can be seen in c and d that the target input frequency develops a plateau as the propagation length is increased. Increasing the propagation length further (panel e) changes the flat-plateau landscape into a hill and a valley. The presence of the plateau as seen in d means that a small range of $\omega_{in}(t)$ will be mapped onto a broad range of $\omega_{out}(t)$ with the desired phase relationships (i.e. chirp). The straight lines in d illustrate this point. First, the bandwidth corresponding to the plateau region ($\Delta\omega_{in}$) is mapped down onto the time axis. This gives us the time duration and the delay of the input pulse, relative to the pump, corresponding to this $\Delta\omega_{in}$ bandwidth. Furthermore, the deviations of $\omega_{in}(t)$ from a perfectly flat plateau define the estimated input chirp (in the time domain). Now, projecting this time interval back onto the vertical axis via the $\omega_{out}(t)$ curve gives us the bandwidth of the output supercontinuum with the desired output chirp. Repeat this same procedure for panels c and e and you will see that a broad output with the desired chirp can not be generated from such a narrow input as seen in d.

Although not stressed in the above analysis, the choice of the pump plays a critical role. The appearance and length of the plateau region are due to the sharply rising central region of the frequency map (Fig. 3a). Lengthening the duration of the pump stretches this region, while shortening the pump shrinks this region. The optimal pump corresponds to the case where the curvature and length of this critical region match the curvature and length of the desired $\Delta\omega_{out}(t)$ region (see panel b). The pump used above has already been optimized using these criteria.

These results can now be used as input into full numerical simulations to 'fine tune' the approximate optimum by perturbing the available parameters to approach the true optimal solution.

3.2   *Full numerical results*

The optimization of the above estimated solution using full numerical simulations proceeds as follows. After using the time-warp analysis to identify an appropriate pump

pulse, propagation length, and pump–probe delay, the target output probe was propagated backwards through the nonlinear medium to obtain the actual input pulse corresponding to this chosen output. The available parameters (propagation length, pump–probe delay, pump and target pulse composition) were then gradually varied until the true optimum (i.e. the narrowest input spectrum leading to the broadest transform-limited output spectrum) was found. It should be stressed that starting from the estimated optimal parameters found via the time-warp analysis greatly reduced the number of numerical test runs required to locate the optimal input parameters.

Figure 4 shows the results of using this full numerical procedure to 'fine tune' the results of the time-warp analysis. The final numerical solution compresses a 66-fs probe at 3 μm (panel a) down to 15 fs at 2.7 μm (panel c). Panel a shows the pump pulse (thin line) and the probe pulse (thick line). Note that the intensities of both pulses have been arbitrarily scaled in the plot (i.e. the probe is not meant to have similar intensity as the pump). The optimal pump–probe delay can then be read from this plot. Panel b shows the input spectrum along with the spectral phase (which requires minimal shaping). Panel d plots the output spectrum and phase, showing that the output is close to transform-limited. The length of the nonlinear medium was 0.85 mm while the length of the additional CaF_2 plate remained at 1.5 mm.

Again using first the time-warp analysis followed by small corrections using the full numerical solution, compression of a probe pulse near 800 nm was modeled. The optimal solution, shown in Fig. 5, compresses a 10.1-fs pulse at 804 nm down to 2.2 fs at 588 nm. The optimized pump pulse used was a single Gaussian with FWHM of 20 fs and is plotted in Fig. 5a. The intensity of the pump was again $n_2 F^2 = 3.2 \times 10^{-3}$ at the maximum of the field. The nonlinear medium used was fused silica and the nonlinear propagation length was $L = 0.15$ mm. No additional glass plate was used in this case for extra compression after the nonlinear medium. Thus, the whole compression can be done in the window of the vacuum chamber.

Table 1 lists a variety of compression results we obtained using this approach. The method is tunable throughout the vis-
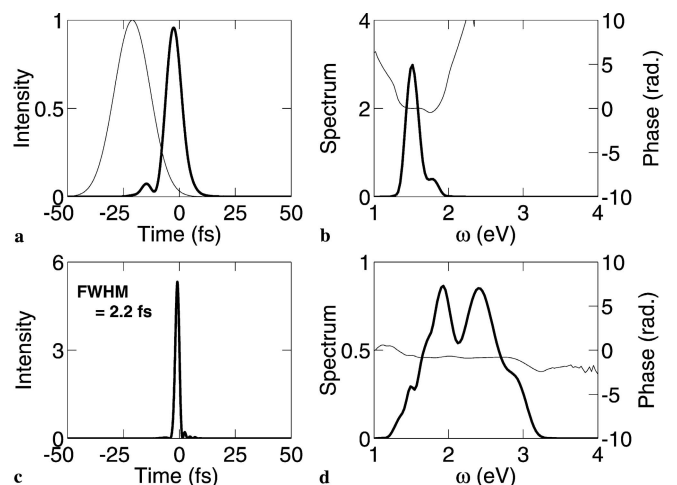

FIGURE 5   As in Fig. 4 but for compression near 800 nm

λ_{in} (nm)	FWHM$_{in}$ (fs)	λ_{out} (nm)	FWHM$_{out}$ (fs)
388	10.1	396	2.7
495	10.0	480	2.4
654	10.0	481	2.8
703	10.2	530	2.6
744	10.0	560	2.3
804	10.1	588	2.2
859	10.0	631	2.6
901	9.95	637	2.5
960	10.0	639	2.7
3000	66.1	2660	14.8

TABLE 1   Tunability of the pump–probe compression

ible and IR. The middle section of the table shows results of compressing input probe pulses of duration 10 fs ranging from 650 to 950 nm down to 2.2–2.8 fs at output wavelengths of 480–640 nm. Each case used a single 20 fs FWHM Gaussian pump at 800 nm as in Fig. 5. The optimal solutions for this wavelength range did not require any additional glass plate after the nonlinear medium. The medium used here was fused silica and had a length of 0.15–0.18 mm.

The results in the first section of the table, for input wavelengths 388 and 495 nm, used a pump pulse with a double-hump structure comprising two Gaussians, the first with FWHM = 25 fs and the second with FWHM = 15 fs, separated by 35 fs. The intensity of the pump was once more $n_2 F^2 = 3.2 \times 10^{-3}$ at the maximum of the field. The nonlinear medium used was CaF$_2$ and the nonlinear propagation length was $L = 0.15$ mm. An additional CaF$_2$ plate of 0.08-mm thickness was used after the nonlinear medium. The optimal pump–probe delay was such that the probe arrived in between the two humps of the pump.

4   Conclusions and outlook

The pulse-compression technique described above appears quite successful in the mid- to near-IR range, where we predict that essentially single-cycle pulses can be generated. As one goes to higher frequencies, towards UV, the quality of compression decreases. The reason is the combination of self-steepening and very strong dispersion: the modification of the pump pulse during propagation gets out of hand.

The problem can be remedied by using hollow-core fibers filled with atomic or molecular gas with low dispersion, such as Ar or N$_2$. Our calculations for pulse compression using rotationally excited molecular gases [14, 15] show that 1-fs pulses in the 'visible' (covering all frequencies from near-IR to UV) are not impossible. The main practical difficulty with using hollow fibers is the need to separate strong pump from weak probe afterwards. The XPM setup presented here, Fig. 1, resolves this problem in a very simple manner.

The main drawback of the method described here is the need to deal with two pulses. Furthermore, it is the weak pulse which is compressed, not the strong one. It would be much more attractive to accomplish the same control over pulse compression using only one pulse, with spectral broadening initiated by SPM.

When dealing with pulse compression using SPM, one has to keep in mind two factors. Firstly, in the time domain SPM would always produce a chirp which changes its sign during the pulse (for a simple case of a single-peaked pulse the chirp will change from negative to positive and back to negative). This naturally prevents dispersion-assisted pulse compression during propagation – such compression requires a fixed sign of the chirp. For example, a down-chirp (negative chirp) is needed for compression in media with normal dispersion. Secondly, in the case of SPM, as with any other self-induced nonlinearity, modification of the input pulse changes the nonlinear response of the medium.

A possible approach to circumventing these difficulties is to have a fixed compressor at the output of the nonlinear medium which would compensate the main part of phase variation in the frequency domain (e.g. quadratic spectral phase). Then one might attempt to compensate the remaining chirp in the time domain by pre-chirping the input pulse, again in the time domain, keeping the amplitude $F_{in}(t)$ of the input field constant (in the frequency domain, this would require amplitude modulation). It remains to be seen whether this approach is viable.

Appendix A: first-order Maxwell equation for weak reflection, without slowly varying envelope approximation

For short pulses – or for pulses with very broad spectra – the usual slowly varying envelope approximation (SVEA) fails. Nevertheless, it is possible (see e.g. [25]) to derive a first-order equation by generalizing the results of [27] for arbitrary media (and not only low-density gases as in [27]). Here, for completeness, we present this derivation. The key approximation in this equation is the assumption of weak reflection. The assumption is valid if the refractive index does not change significantly over a wavelength, which is a typical case. The derivation follows [25]. For simplicity, we restrict ourselves to a 1D case.

The Maxwell equation in 1D is

$$\frac{\partial^2 E}{\partial x^2} - \frac{1}{c^2}\frac{\partial^2 E}{\partial t^2} = \frac{4\pi N}{c^2}\frac{\partial^2 P}{\partial t^2}. \tag{A.1}$$

Here N is number density and P is polarization per unit particle, i.e. induced dipole per quantum system. The density will soon be absorbed into the refractive index.

Fourier transforming, we get

$$\frac{\partial^2 E(\omega)}{\partial x^2} + \frac{\omega^2}{c^2} E(\omega) = -\frac{4\pi N}{c^2}\omega^2 P(\omega), \tag{A.2}$$

and the next step towards a first-order equation is to write the polarization P as a sum of the linear and nonlinear terms:

$$P(\omega) = \chi(\omega) E(\omega) + P_{NL}(\omega). \tag{A.3}$$

The linear part is moved onto the left-hand side, yielding

$$\left(\frac{\partial^2}{\partial x^2} + \frac{\omega^2}{c^2}(1 + 4\pi N\chi(\omega))\right) E(\omega) = -\frac{4\pi N}{c^2}\omega^2 P_{\mathrm{NL}}(\omega) .$$

$$(A.4)$$

Now we can get rid of the number density N and introduce the linear refractive index of the medium,

$$n^2(\omega) = 1 + 4\pi N\chi(\omega) . \qquad (A.5)$$

With this substitution, the wave equation looks like

$$\left[\frac{\partial^2}{\partial x^2} + \frac{\omega^2}{c^2}n^2(\omega)\right] E(\omega) = -\frac{4\pi N}{c^2}\omega^2 P_{\mathrm{NL}}(\omega) . \qquad (A.6)$$

Finally, to prepare for the approximation ahead, we re-write the square brackets as

$$\left[\frac{\partial}{\partial x} + i\frac{\omega}{c}n(\omega)\right]\left[\frac{\partial}{\partial x} - i\frac{\omega}{c}n(\omega)\right] E(\omega) = -\frac{4\pi N}{c^2}\omega^2 P_{\mathrm{NL}}(\omega) . \qquad (A.7)$$

So far, we have made no approximations whatsoever. Now comes the most critical one: we assume that the electric field is mostly propagating in one direction. Here is how it comes into play.

For the right-propagating wave the convention is:

$$E(\omega, x) \propto e^{-i\omega t + ik(\omega)x} , \qquad (A.8)$$

where the wavenumber k is

$$k(\omega) = \frac{\omega}{c}n(\omega) . \qquad (A.9)$$

Therefore, if the waves are mostly right-propagating, in zero order

$$\frac{\partial}{\partial x}E(\omega, x) \approx ik(\omega)E(\omega, x) = i\frac{\omega}{c}n(\omega)E(\omega, x) . \qquad (A.10)$$

This is the zero-order approximation. If we now put it back into each of the square brackets in (A.7), we will get nonsense: zero on the left-hand side, due to the zero in the second square bracket.

But, in the first approximation, we can keep the small term in the second square bracket

$$\frac{\partial}{\partial x}E(\omega, x) - i\frac{\omega}{c}n(\omega)E(\omega, x) \qquad (A.11)$$

intact while dropping this small term in the other square bracket:

$$\frac{\partial}{\partial x}E(\omega, x) + ik(\omega)E(\omega, x)$$
$$= 2ik(\omega)E(\omega, x) + \left(\frac{\partial}{\partial x}E(\omega, x) - ik(\omega)E(\omega, x)\right)$$
$$\approx 2ik(\omega)E(\omega, x) . \qquad (A.12)$$

This is, in fact, the only approximation we need. It includes the reflected wave in first order by keeping it exactly in the second

square bracket in (A.7), but dropping the reflected wave in the first square bracket where a big term is sitting beside it.

This simple trick kills one space derivative. Now the equation is

$$\left[\frac{\partial}{\partial x} - i\frac{\omega}{c}n(\omega)\right] 2\frac{n(\omega)}{c}i\omega E(\omega) = -\frac{4\pi N}{c^2}\omega^2 P_{\mathrm{NL}}(\omega) . \quad (A.13)$$

Crossing out ω/c on both sides, we effectively get rid of one time derivative to add to one of the space derivatives that has disappeared a moment earlier. We have

$$\left[\frac{\partial}{\partial x} - i\frac{\omega}{c}n(\omega)\right] E(\omega) = \frac{2\pi N}{cn(\omega)}i\omega P_{\mathrm{NL}}(\omega) . \qquad (A.14)$$

REFERENCES

1 G.P. Agrawal: *Nonlinear Fiber Optics* (Academic, San Diego 1995)
2 R.W. Boyd: *Nonlinear Optics* (Academic, San Diego 1992)
3 Although the slowly varying envelope approximation breaks down near the single-cycle regime, previous analytical studies of relevance to the present work have used this approximation to show the potential for pulse compression by XPM. See e.g. E.M. Dianov, P.V. Mamyshev, A.M. Prokhorov, S.V. Chernikov: Kvant. Elektron. **15**, 1941 (1988); A.M. Zheltikov, N.I. Koroteev, A.N. Naumov: JETP **88**, 857 (1999)
4 C.G. Durfee III, S. Backus, H.C. Kapteyn, M.M. Murnane: Opt. Lett. **24**, 697 (1999)
5 A.V. Sokolov, D.R. Walker, D.D. Yavuz, G.Y. Yin, S.E. Harris: Phys. Rev. Lett. **87**, 033 402 (2001); Phys. Rev. Lett. **85**, 562 (2000)
6 N. Zhavoronkov, G. Korn: Phys. Rev. Lett. **88**, 203 901 (2002) and references therein
7 R.A. Bartels, T.C. Weinacht, N. Wagner, M. Baertschy, C.H. Greene, M.M. Murnane, H.C. Kapteyn: Phys. Rev. Lett. **88**, 013 903 (2002)
8 R.L. Fork, C.H. Brito Cruz, P.C. Becker, C.V. Shank: Opt. Lett. **12**, 483 (1987)
9 A. Baltuška, Z. Wei, M.S. Pshenichnikov, D.A. Wiersma: Opt. Lett. **22**, 102 (1997)
10 M. Nisoli, S.D. Silvestri, R. Szipocs, K. Ferencz, C. Spielmann, S. Sartania, F. Krausz: Opt. Lett. **22**, 522 (1997)
11 A. Baltuška, T. Fuji, T. Kobayashi: Opt. Lett. **27**, 306 (2002)
12 A.M. Weiner: Prog. Quantum Electron. **19**, 161 (1995)
13 F. Verluise, V. Laude, Z. Cheng, C. Spielmann, P. Tournois: Opt. Lett. **25**, 575 (2000)
14 V. Kalosha, M. Spanner, J. Herrmann, M.Y. Ivanov: Phys. Rev. Lett. **88**, 103 901 (2002)
15 M. Spanner, M. Ivanov: Opt. Lett. **28**, 576 (2003)
16 The propagation would have been completely linear if it were not for the interplay between spectral broadening and dispersion: spectral broadening feeds into dispersion which changes the pulse. This, in turn, affects further spectral broadening which affects dispersion, and so on
17 M. Spanner, M.Y. Ivanov, V. Kalosha, J. Herrmann, D. Wiersma, M. Pshenichnikov: Opt. Lett. **28**, 749 (2003)
18 C.J. Bardeen, V.V. Yakovlev, K.R. Wilson, S.D. Carpenter, P.M. Weber, W.S. Warren: Chem. Phys. Lett. **280**, 151 (1997)
19 R. Bartels, S. Backus, E. Zeek, L. Misoguti, G. Vdovin, I.P. Christov, M.M. Murnane, H.C. Kapteyn: Nature **406**, 164 (2000)
20 R.S. Judson, H. Rabitz: Phys. Rev. Lett. **68**, 1500 (1992)
21 A. Assion, T. Baumert, M. Bergt, T. Brixner, B. Kiefer, V. Seyfried, M. Strehle, G. Gerber: Science **282**, 919 (1998)
22 T.C. Weinacht, J.L. White, P.H. Bucksbaum: J. Phys. Chem. A **103**, 10 166 (1999)
23 R.J. Levis, G.M. Menkir, H. Rabitz: Science **292**, 709 (2001)
24 F.G. Omenetto, A.J. Taylor, M.D. Moores, D.H. Reitze: Opt. Lett. **26**, 938 (2001)
25 See e.g. J. Herrmann, U. Griebner, N. Zhavoronkov, A. Husakou, D. Nickel, J.C. Knight, W.J. Wadsworth, P.S.J. Russell, G. Korn: Phys. Rev. Lett. **88**, 173 901 (2002); A.V. Husakou, J. Herrmann: Phys. Rev. Lett. **87**, 203 901 (2001)
26 V.P. Kalosha, J. Herrmann: Phys. Rev. Lett. **85**, 1226 (2000)
27 R.K. Bullough, P.M. Jack, P.W. Kitchenside, R. Saunders: Phys. Scr. **20**, 364 (1979)